IEEE Photonics Journal
An IEEE Photonics Society Publication

Open Access

A Band Enhanced Plasma Metamaterial Absorber Based on Triangular Ring-Shaped Resonators

Volume 10, Number 4, August 2018

Hai-Feng Zhang
Hao Zhang
Yi Yao
Jing Yang
Jia-Xuan Liu

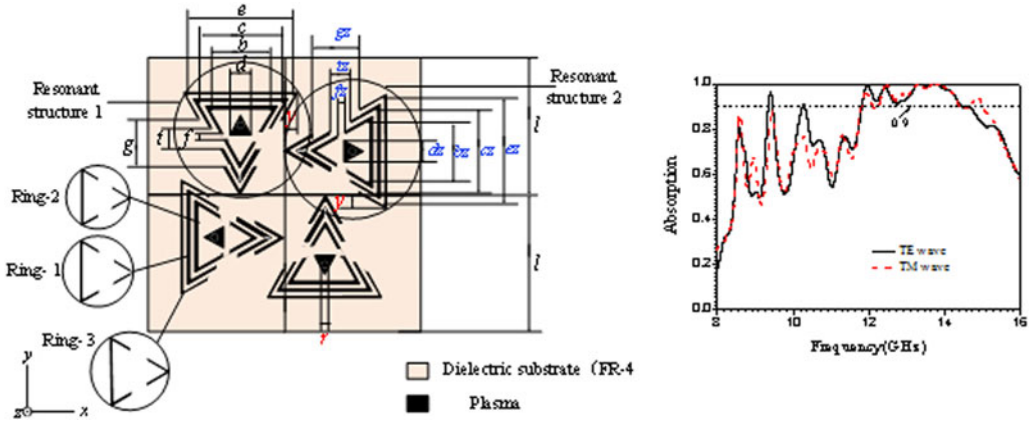

DOI: 10.1109/JPHOT.2018.2854906
1943-0655 © 2018 IEEE

IEEE photonics SOCIETY

IEEE

A Band Enhanced Plasma Metamaterial Absorber Based on Triangular Ring-Shaped Resonators

Hai-Feng Zhang,[1] **Hao Zhang**,[1] **Yi Yao**,[2] **Jing Yang**,[1] **and Jia-Xuan Liu**[1]

[1]College of Electronic and Optical Engineering and College of Microelectronics, Nanjing University of Posts and Telecommunications, Nanjing 210023, China
[2]School of Mathematical Sciences, Nanjing Normal University, Nanjing 210023, China

DOI:10.1109/JPHOT.2018.2854906

Manuscript received June 14, 2018; revised July 3, 2018; accepted July 6, 2018. Date of publication July 11, 2018; date of current version July 30, 2018. This work was supported in part by the Major Program of National Natural Science Foundation of China under Grants 71690242 and 91546118; in part by the China Postdoctoral Science Foundation under Grant 2013M541697; and in part by the Postdoctoral Foundation of Jiangsu Province under Grant 1302044C. Corresponding author: Y. Yao (e-mail: 05302@njnu.edu.cn).

Abstract: In this paper, a novel way is proposed to realize a broadband absorber, which is based on the plasma metamaterial with the triangular ring-shaped resonators. Each unit cell of the proposed absorber includes three layers, which are metal layer, dielectric layer, and solid-state plasma (SSP) layer, respectively. The top layer is composed of the truncated SSP triangular ring-shaped resonators and the SSP triangular patches, which are situated the middle of triangular rings. An SSP cylinder also is inserted between the central of each SSP triangular patch and the bottom metal layer. The absorption bandwidth can be covered from 11.76 to 14.43 GHz when the absorption rate is larger than 90%, which also is polarization-independent. In addition, the better performances can be realized under different incident angles. To explain the mechanism of high absorption, the electric field, the surface current distribution, and power loss density at different resonant frequencies are present. Moreover, the tunable absorption can be obtained in the proposed absorber while the performance of the absorber can be improved by exciting the different SSP resonators.

Index Terms: Absorber, plasma metamaterials, tunability.

1. Introduction

Metamaterials can be considered as the artificial electromagnetic atoms or molecules, which have many unique properties not found in nature, such as negative permittivity [1], and negative refractive index [2]. In recent years, metamaterials have attracted considerable research attention due to the designable and controllable material parameters in the design of artificial metamaterial resonators. With the continuous investigations on electromagnetic metamaterials, many exotic properties of metamaterials have been revealed and applied, which comprise perfect lens [3], perfect absorber [4], invisibility cloak [5], etc.

As an aspect for the important application of metamaterials, metamaterial absorbers (MA) are of great interest for the communities of both physics and material science and have found an increasingly wide utilization in many fields including photodetectors [6], energy harvesting [7], and

solar cells [8]. Since the MA with near unity absorbance was presented by Landy [9] *et al.* many different types of MAs are designed in diverse frequency ranges, such as microwaves [10], terahertz [11], infrared [12], and optical regions [13]. Most MAs can only operate at rather narrow frequency region. For the practical applications, the broadband absorbers are more valuable. Therefore, many methods of broadening the absorption band are proposed. For instant, a novel three-dimensional MA with eight-fold rotational symmetry was created by Dong [14] *et al.* which shown that the polarization-insensitive absorption is over 90% at 26.9–32.9 GHz. Hoa [15] *et al.* utilized a periodic array of metallic-dielectric multilayered conical frustums to devise a wide-angle and polarization-independent broadband absorber, which exhibits a broadband absorption performance with the absorption rate exceeding 90% from 10.8 GHz to 15.8 GHz. A wideband and polarization-insensitive absorber based on lumped resistors was presented by Li [16] *et al.*, and 9.25 GHz-wide absorption from 7.93 GHz to 17.18 GHz with absorption above 90% can be obtained. In addition, other absorbers also were proposed, such as engineering the frequency dispersion of metamaterial surface [17], some special material [18], or using the high-impedance surface [19], for realizing the broadband absorption.

On the other hand, the designed antennas using a gaseous plasma have been successfully developed for the first time in 1998 [20]. Afterwards, numerous major research results were revealed. However, gaseous plasma has great limitations in engineering applications due to many properties. In this paper, solid state plasma (SSP) is gradually applied to the design of the absorber. And SSP as a novel metamaterial gradually has been attracting great interest due to many excellent properties [21]–[23], which can realized by GaAs [21], [22] and S-PIN [23]. The conductivity of SSP will increase with the increase of carrier concentration, when the carrier concentration reaches a certain value. It means that the properties of SSP can be analogous to the metal. Therefore, the tunable absorption spectra can be obtained in the plasma metamaterial absorber (PMA) through exciting different regions of SSP resonators.

The aim of this paper is to propose a novel way to achieve the broadband absorber based on the plasma metamaterial with triangular ring-shaped resonators in theory. The absorption rate of proposed broadband PMA spans from 11.76 GHz to 14.43 GHz, which is over 90%. And such a broadband PMA can realize a wide angle of incidence. Moreover, the electric field, surface current distribution and the power loss density are calculated to analyze the absorption mechanism. In addition, the tunable absorption can be acquired in the proposed PMA, and the performance of such an absorber can be improved by exciting the different SSP resonators. In this paper, we consider the SSP is realized by GaAs [21], [22]. How to fabricate such an absorber and do experimental verification are beyond the scope of this paper.

2. Design and Simulation

The schematic views of four PMAs and their corresponding absorption spectrum are depicted in Figs. 1–4 and Figs. 5(a)–(d), respectively. It is noted that all PMAs are composed of three layers and copper with an electric conductivity of 5.8×10^7 S/m is adopted on the bottom layer. The permittivity of the SSP resonators is described by the Drude model, which can be expressed as $\varepsilon_p(\omega) = \varepsilon_\infty - {\omega_p}^2/(\omega^2 + j\omega\omega_c)$ [21], [22]. Based on the results in Refs. [21], [22], we consider $\varepsilon_\infty = 12.8$, the plasma frequency is $\omega_p = 2.9 \times 10^{14}$ rad/s and the collision frequency is $\omega_c = 1.65 \times 10^{13} 1/s$. The efficiency of absorber is characterized as $A(\omega) = 1 - R(\omega) - T(\omega)$, where $A(\omega)$ is the absorptivity and $R(\omega)$ and $T(\omega)$ are the reflectivity and transmission. Due to the copper plate used as the backplane of the PMA, the transmission coefficient is zero. Thus, the expression of $A(\omega)$ can be simplified as $A(\omega) = 1 - R(\omega)$. In following, all of the results are calculated by the commercial simulation software HFSS 13.

The front and the side views of a dual-band PMA is displayed in Fig. 1, which show that the upper layer consists of a truncated SSP triangular ring-shaped and a triangular patch resonators and the dielectric substrate is selected to be SiO_2 with the relative permittivity of $\varepsilon = 2.1 + i0.02$. In order to calculate, for each unit cell, the both sides of x or y directions are set to periodic boundary conditions

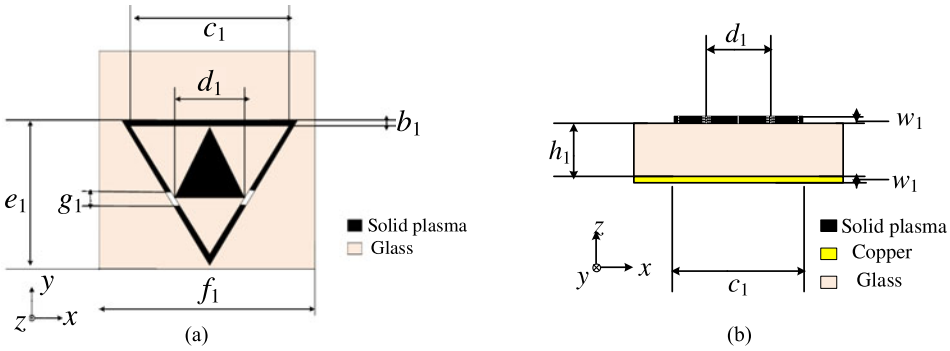

Fig. 1. Schematic views of the unit cell for the dual-band PMA. (a) the front view l, and (b) the side view, the dimensions are $b_1 = 0.8$ mm, $c_1 = 18.23$ mm, $d_1 = 9.11$ mm, $f_1 = 24.23$ mm, $g_1 = 1.6$ mm, $h_1 = 3$ mm, $w_1 = 0.0138$ mm.

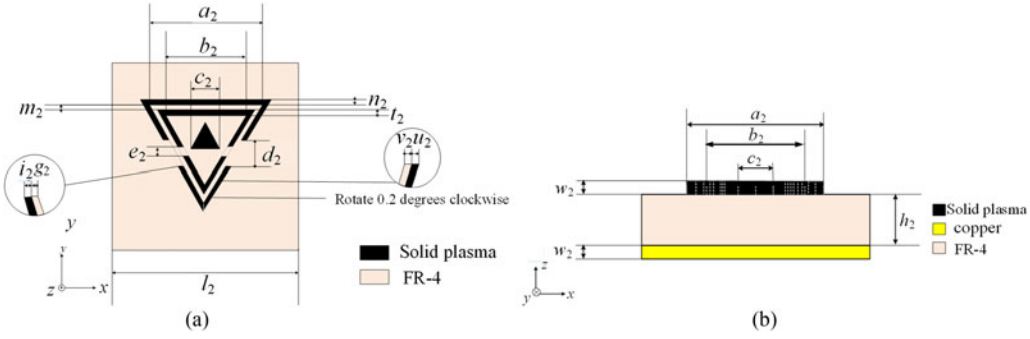

Fig. 2. Schematic views of the unit cell for the narrow band PMA. (a) the front view of unit cell, and (b) the side view of unit cell, the dimensions are $a_2 = 49.44$ mm, $b_2 = 43.2$, $c_2 = 18.6$ mm, $d_2 = 8.7$ mm, $m_2 = 0.8$ mm, $n_2 = 1.8$ mm, $i_2 = 1.2$ mm, $t_2 = 1$ mm, $l_2 = 72$ mm, $g_2 = 0.9$ mm, $v_2 = 0.9$ mm, $u_2 = 57.75$ mm, $e_2 = 2$ mm, $k_2 = 1.5$ mm, $h_2 = 2.9$ mm, $w_2 = 0.04$ mm.

in HFSS 13. The absorption spectrum of such a dual-band PMA is plotted in Fig. 5(a), which reveals that there are two strong peaks at 9.49 GHz and 10.62 GHz with the absorption of about 99.92% and 99.4%, respectively. If we want to obtain a wider bandwidth of absorption, such a PMA has to be modified. Thus, a narrow band PMA is proposed in Fig. 2, which consists of two truncated triangular ring-shaped and a triangular patch resonators (SSP) on the surface of the dielectric substrate. The dielectric substrate is made of lossy FR4, whose relative permittivity is 4.3 and the loss tangent is 0.025. The absorption spectrum of such a narrow-band PMA is given in Fig. 5(b). As shown in Fig. 5(b) that the frequency ranges of absorption exceed 90% are covered from 9.28 GHz to 9.45 GHz and 11.21 GHz to 11.37 GHz. Similarly, if an additional SSP truncated triangular ring-shaped resonator is added on such a narrow-band PMA, a new PMA can be achieved. The schematic views and simulated result are plotted in Figs. 3 and 5(c), respectively. As shown in Fig. 5(c), the absorption rate runs from 9.28 GHz to 9.59 GHz, and 11.3 GHz to 11.46 GHz, which is over 90%. Compared Fig. 5(c) with Fig. 5(b), the absorption bandwidth is enhanced obviously. However, the PMA as described in Fig. 3 is polarization-dependent and its absorption bandwidth is narrow. If we want to realize a broadband PMA, a new designing has to be done. In Fig. 4, the schematic views of a broadband PMA are plotted. For such a PMA, the lossy FR4 is used as the dielectric substrate, and its unit cell contains four truncated SSP triangular ring-shaped and triangular patch resonators on the top layer, which are oriented in different directions and the same size on the diagonal. It is noticed that there is a inserted SSP cylinder with radius r between the central of each SSP triangular patch and the bottom layer. It can be observed from Fig. 5(d) that, for TE

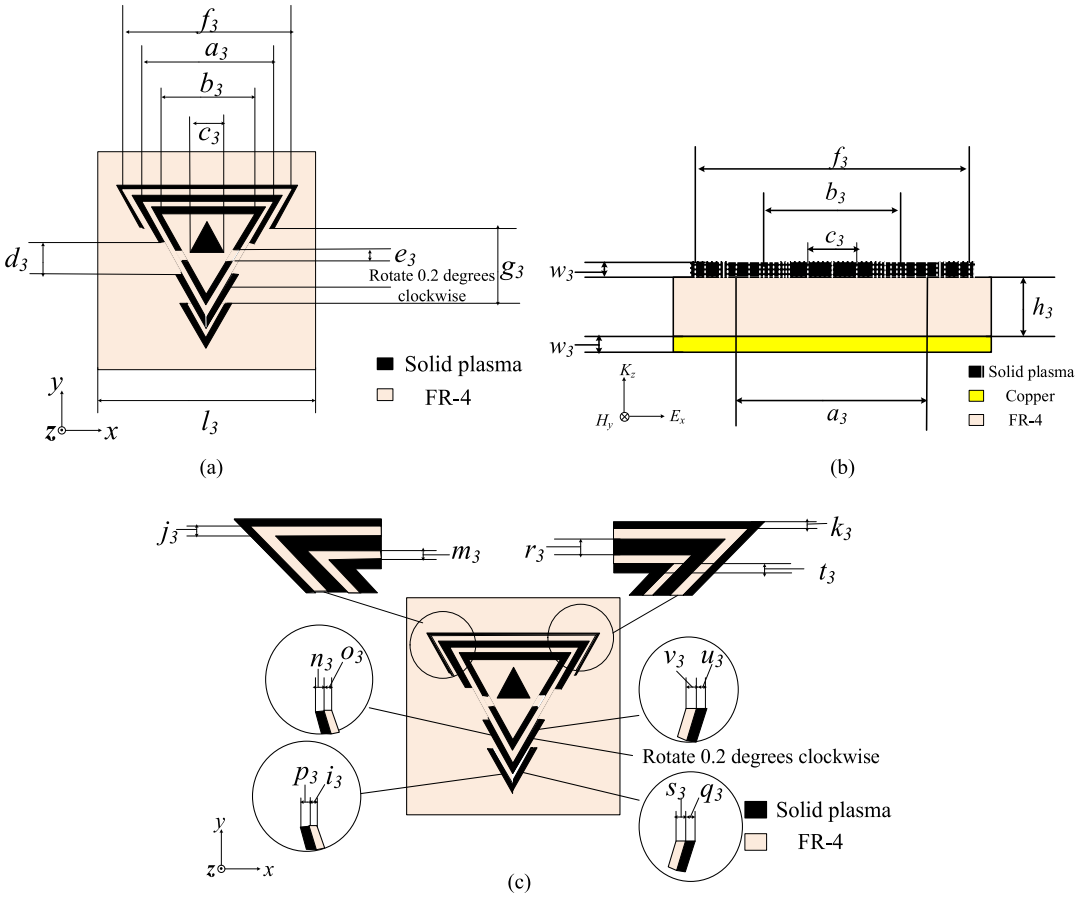

Fig. 3. Schematic views of the unit cell for the narrow band enhanced PMA. (a) the front view of unit cell, (b) the front view of unit cell, and (c) the side view of unit cell, the dimensions are $a_3 = 49.44$ mm, $b_3 = 43.2$ mm, $c_3 = 18.6$ mm, $d_3 = 9.11$ mm, $e_3 = 2$ mm, $f_3 = 57.75$ mm, $g_3 = 18.03$ mm, $h_3 = 2.9$ mm, $i_3 = 1$ mm, $j_3 = 0.7$ mm, $k_3 = 0.08$ mm, $l_3 = 72$ mm, $m3 = 0.8$ mm, $n_3 = 1.2$ mm, $o_3 = 1.1$ mm, $p_3 = 1.2$ mm, $q_3 = 1.5$ mm, $r_3 = 1.7$ mm, $s_3 = 0.5$ mm, $t_3 = 1$ mm, $u_3 = 1.2$ mm, $v_3 = 1$ mm, $w_3 = 0.04$ mm.

wave, the absorption rate above 90% covered frequency range of 11.76–14.43 GHz. For TM wave, the corresponding frequency range is 12.21–14.41 GHz. As we know, the SPP is one kind of tunabe material, and its plasma frequency can be adjusted by the external voltage. Based on the results in Refs. [21], [22], the plasma frequency of GaAs is proportional to the external voltage within a certain voltage range. In Fig. 5(e), absorption spectra vs. different plasma frequencies are plotted. As shown in Fig. 5(e), for TE wave, when $\omega_p = 2.9 \times 10^{12}$ and 2.9×10^{10}, respectively, the absorption features of the proposed PMA will deteriorate. Thus, the external voltage has to be a larger value to obtain a a broadband absorption.Obviously, a broadband PMA can be obtained by the designing processes as mentioned above. In the other word, a broadband PMA can be realized by arranging the narrow band PMAs with 90 degree rotational symmetry, and such a broadband PMA also is polarization-dependent. In the practical applications, we can use the finite periodic structure to replace the theoretical model (an infinite number of periodic unit cells).

To illustrate the properties of the present broadband PMMA, the absorption spectra of different excited plasma resonators are shown in Fig. 6. It can be seen from Fig. 6(a) that when all of the “ring-1” solid plasma resonators [see Fig. 4(c)] are excited, the absorption goes beyond 90% from 13 to 13.24 GHz. When both “ring-1” and “ring-2” solid plasma resonators are excited, the absorption spectrum is plotted in Fig. 6(b). As shown in Fig. 6(b), the absorption rate are 90% at 13.03–14.34 GHz. Then, in Fig. 6(c), the broadband PMMA exhibits an absorption performance

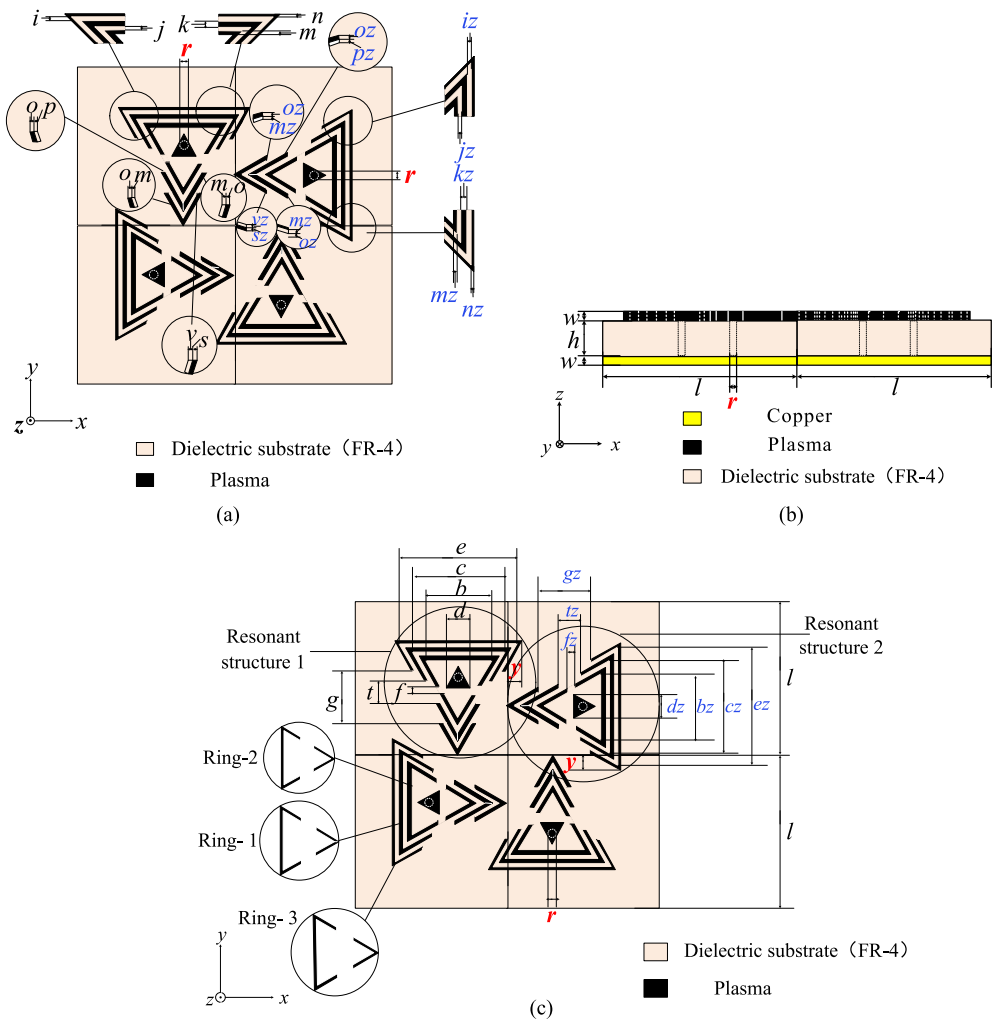

Fig. 4. Schematic views of the unit cell for the broadband PMA. (a) the front view of unit cell, (b) the side view of unit cell, and (c) the front view of unit cell, the dimensions are $b = 21.6$ mm, $c = 24.71$ mm, $d = 9.3$ mm, $e = 27.87$ mm, $f = 1$ mm, $g = 9.16$ mm, $h = 2.9$ mm, $i = 0.35$ mm, $j = 0.4$ mm, $k = 0.85$ mm, $l = 18$ mm, $m = 0.5$ mm, $n = 0.04$ mm, $o = 0.6$ mm, $p = 0.55$ mm, $r = 1.5$ mm, $s = 0.75$ mm, $t = 5.15$ mm, $v = 0.25$ mm, $w = 0.1$ mm, $y = 4.6$ mm, $z = 0.98$ time.

with the absorptivity larger than 90% which is covered 13.03–14.34 GHz, when all of the plasma resonators are excited. Compared the results in Fig. 6(c) with those in Fig. 6(a) and (b), the absorption bandwidth of the proposed broadband PMMA is broadened apparently when all of the plasma resonators are excited. It can be concluded that not only the tunable absorption can be obtained in the proposed PMMA but also the performance of the absorber can be improved by exciting different plasma resonators based on those results as mentioned above

3. Theoretical Analysis

In order to figure out the physical mechanism of the proposed broadband PMA, the electric fields at cross-section of 2.89 mm and the distributions of surface current for two resonance frequencies (11.96 GHz and 13.73 GHz) are calculated, respectively. As shown in Fig. 7(a) and (c), the electric field intensities are distributed in the dielectric substrate at 11.96 GHz and 13.73 GHz (see the locations marked "○"). We can know that the obtained broadband absorption of the PMA is due

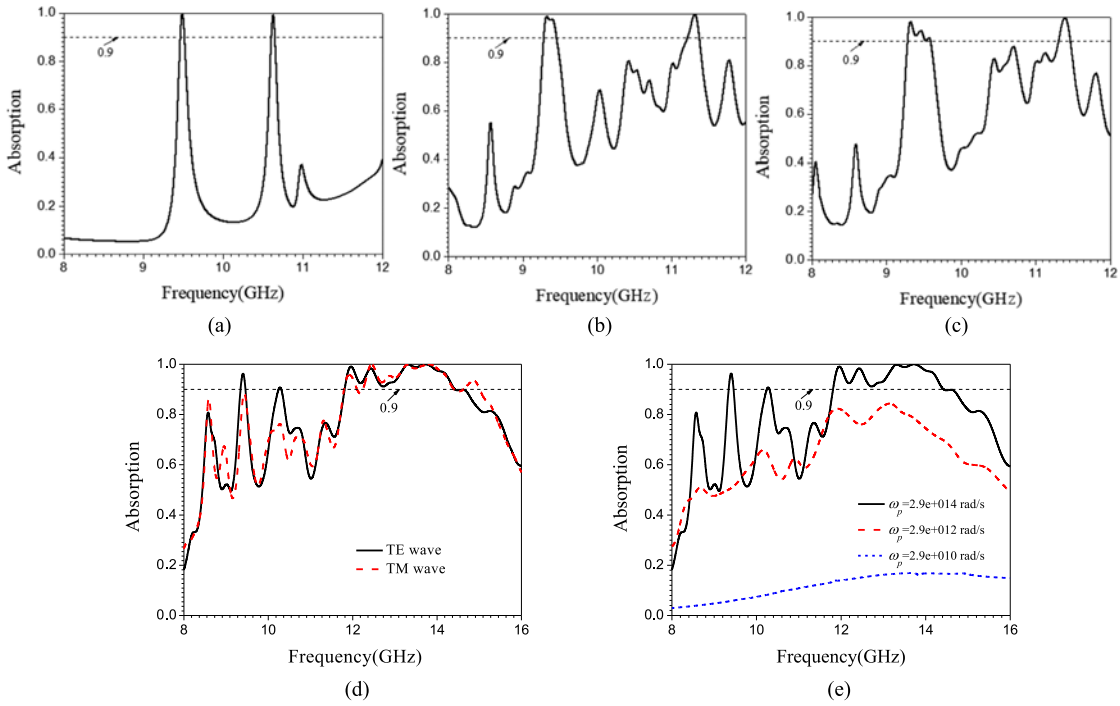

Fig. 5. Absorption spectra of the different PMA. (a) absorption spectrum of the dual-band PMA, (b) absorption spectrum of the narrow band PMA, (c) absorption spectrum of the enhanced narrow band PMA, (d) absorption spectrum of the broadband PMA, and (e) absorption spectra of different plasma frequencies.

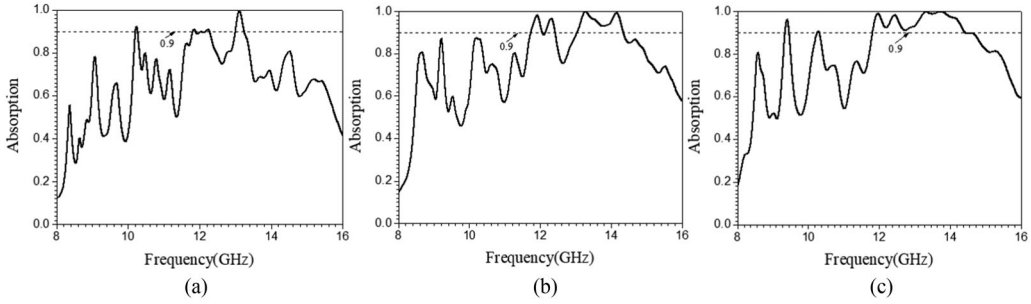

Fig. 6. Absorption spectra of the broadband PMA with exciting different solid plasma resonator.s (a) all of "ring-1" resonators excited, (b) both "ring-1" and "ring-2" plasma resonators excited, and (c) all of the plasma resonators excited.

to dielectric resonances of dielectric substrate. The electromagnetic energy is consumed in the dielectric substrate (lossy FR4) when the incident electromagnetic wave propagates through the SSP resonators. We can observe from Fig. 7(a) that the electric fields are mainly localized the edge of the triangular rings and the middle of the triangular patch (see the locations marked "○"). Such a phenomenon can be reckoned as a positive charge located on the surface of the dielectric substrate. As shown in Fig. 7(b), the surface currents on the reflector (bottom layer) flow in the direction of the arrows, which can be equivalent to a negative charge situated the bottom layer. As mentioned above, the upper and bottom surfaces can be viewed as a electric dipole exhibiting magnetic resonances. The similar physical mechanism also can be obtained in Fig. 7(c) and (d). Therefore, such an absorption phenomenon is caused by the dielectric and magnetic resonances.

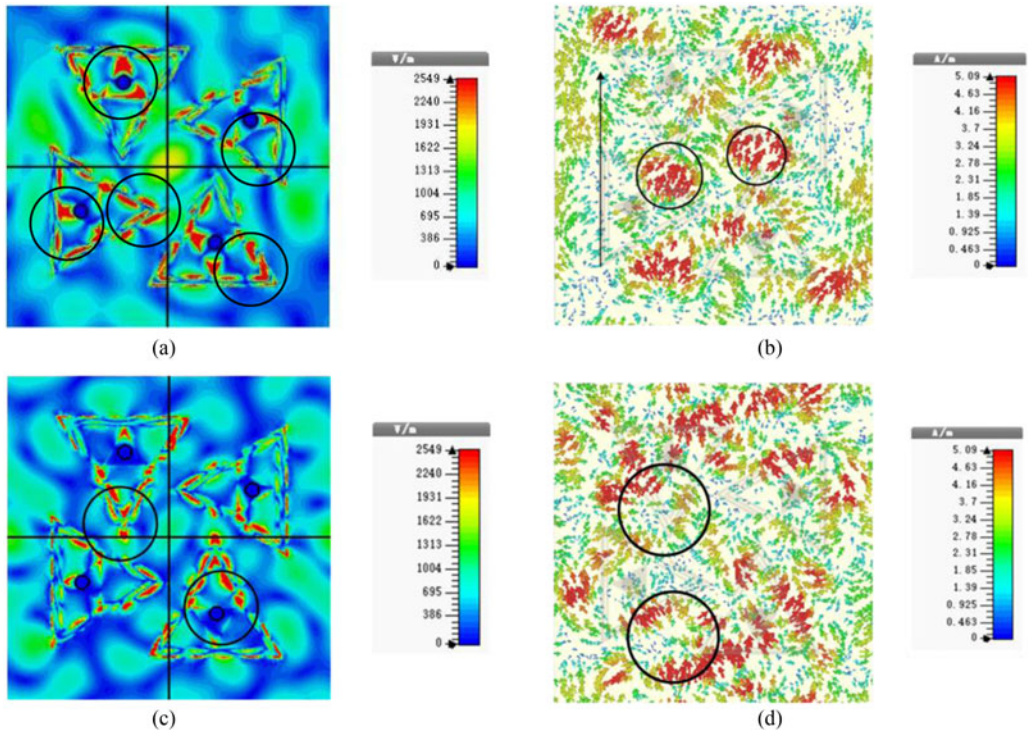

Fig. 7. The electric fields and the backplane surface current distributions at the different resonant frequencies. (a) the electric field distribution at 11.96 GHz, (b) the backplane surface current distribution at 11.96 GHz, (c) the electric field distribution at 13.73 GHz, and (d) the backplane surface current distribution at 13.73 GHz.

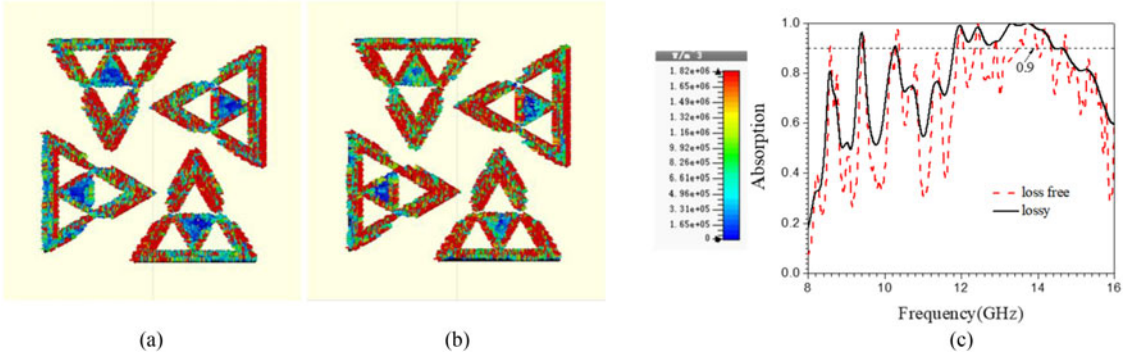

Fig. 8. The power loss density at the different resonant frequencies and the spectra of the dielectric substrate with different loss. (a) the power loss density at 11.96 GHz, (b) the power loss density at 11.73 GHz, (c) the spectra of the dielectric substrate with different loss.

The power loss density and the different absorption spectra when the dielectric substrate (FR4) is lossy and loss free are plotted in Fig. 8. The power loss density in the surface of SSP resonators at 11.96 GHz and 13.73 GHz are shown in Fig. 8(a) and (b), respectively. We can see from Fig. 8(a) and (b) that the power loss density are mainly distributed in the edge of triangular ring-shaped resonators, and the power loss density at 13.73 GHz is much stronger than that at 11.96 GHz, which means that more electromagnetic energy is consumed in the high frequency. It can be seen from Fig. 8(c) that there are only four strong peaks in frequency region 12–14.5 GHz when the dielectric substrate (FR4) is loss free. Obviously, the absorption performance of PMA is

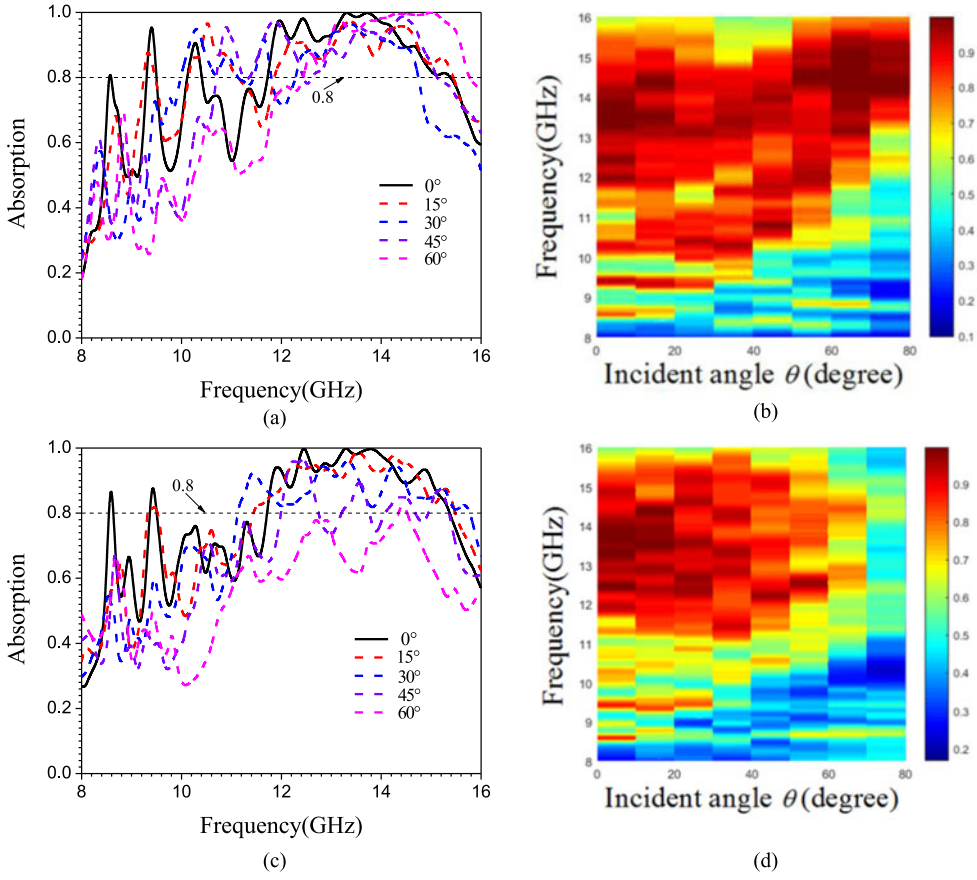

Fig. 9. Absorption spectra and frequency dependence of absorption with different incident angles for TE and TM waves. (a) absorption spectrum for $\theta = 0^\circ$, 15°, 30°, 45° and 60° for TE wave, (b) frequency dependence of absorption under different incident angles for TE wave, (c) absorption spectrum for $\theta = 0^\circ$, 15°, 30°, 45° and 60° for TM wave, and (d) frequency dependence of absorption under different incident angles for TM wave.

decreased. Hence, the energy of incident electromagnetic wave is consumed by SSP resonators and dielectric substrate.

In Fig. 9, the spectra are also computed to study the independence of incident angles for TE and TM waves. It can be seen from Fig. 9(a) that, for TE wave, the absorption is basically kept above 80% in frequency region 12–15 GHz when the incident angle θ is changed from 0° to 60°. As shown in Fig. 9(c), the frequency region of the absorption coefficient over 90% is covered from 11.71 GHz to 15.37 GHz when the incident angleθ is less than 30°. However, the absorption rate merely goes beyond 59% for the incident angle of 60°. The frequency dependence of the absorption under different incident angles are also displayed in Fig. 9(b) and (d). For TE wave, the absorption effect is still significant when θ is up to 70°. However, for TM wave, the absorption rate is slightly decreased when the value of incident angle θ is increased from 40° to 80°. As mentioned above, we can know that, for TE wave, the higher absorption can be achieved under the wider incident angles in the proposed broadband PMA.

The relationships between the absorption of the proposed broadband PMA and the parameters r (the radius of inserted solid plasma cylinder as shown in Fig. 4) and y are illustrated in Fig. 10. As shown in Fig. 10(a), when the value of r is increased, the absorption is basically unaltered in frequency region of 12–14.5 GHz. However, near resonance frequency $f_1 = 13.04$ GHz, the absorption is decreases slightly, whose value is decreased to 88.9% ($r = 2.1$ mm). In Fig. 10(b), the dependence of the absorption spectra with different parameter r are depicted. It can be seen from

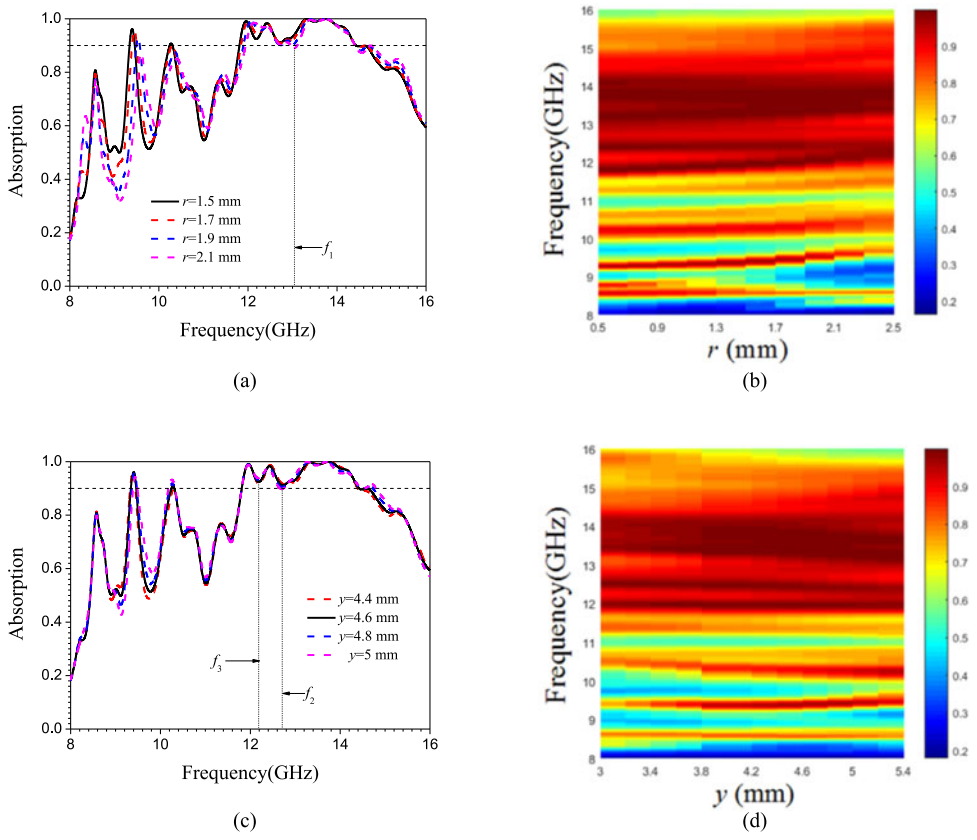

Fig. 10. The absorption spectra and frequency dependence of absorption with different geometric parameters. (a) the absorption spectrum for different parameter *r*, (b) the frequency dependence of absorption for different parameter *r*, (c) the absorption spectrum for different parameter *y*, and (d) the frequency dependence of absorption for different parameter *y*.

Fig. 10(b) that the frequency region of absorption shifts the higher frequencies obviously, when the value of *r* is increased from 0.5 to 2.5 mm. Similarly, the relationships between the absorption and parameter *y* are displayed in Fig. 10(c) and (d). The initial value of the parameter *y* is set to 4.6 mm. In Fig. 10(c), the absorption spectra of $y = 4.4, 4.6, 4.8, 5$ mm are plotted, respectively. One can see from Fig. 10(c) that if the value of *y* is increased, the absorption will be changed at the resonance frequencies $f_2 = 12.72$ GHz and $f_3 = 12.16$ GHz. It also can be seen from Fig. 10(c) that if $y = 5$ mm, the value of absorption will be decreased to 89.71% at resonance frequency f_3, and the frequency range of absorption higher than 90% also is narrowed. As shown in Fig. 10(d), if the value of *y* is increased from 3 to 5.4 mm, the frequency region of absorption will shift lower frequencies. As mentioned above, the parameters *r* and *y* are the important parameters to realize the proposed broadband PMA. If we want to obtain a broadband absorption, the values of *r* and *y* have to be optimized.

It is worth noting that another geometric shapes also can be used to realized the SPP resonators of the proposed PMA except for triangular shape, such as hexagonal and rectangular etc. The similar results also can be obtained.

4. Conclusion

In summary, the designing processes broadband PMA based on the SSP is proposed, and a broadband PMA also is realized. The SSP is realized by GaAs. The configuration of unit cell for the proposed PMA is that the truncated SSP triangular ring-shaped resonators and the SSP triangular

patches are placed on the surface of substrate, and there exists a inserted SSP cylinder between the central of each SSP triangular patch and the bottom layer. The proposed broadband PMA can maintain 90% absorptivity in the frequency range of 11.76–14.43 GHz, and also is polarization-insensitive due to the symmetrical arrangement of the resonators. If the incident angle is less than 60°, the polarization-insensitive broadband absorption can be achieved. The calculated results also demonstrated that the tunable absorption spectra can be obtained by exciting different SSP resonators, whose absorption coefficient is larger than 90%. Thus, such designing processes of PMA offers a valuable way to realize a polarization-independent and tunable broadband absorber.

References

[1] J. Pendry, A. Holden, W. Stewart, and I. Youngs, "Extremely low frequency plasmons in metallic mesostructure," *Phys. Rev. Lett.*, vol. 76, pp. 4773–4776, 1996.

[2] Z.-J. Wong *et al.*, "Optical and acoustic metamaterials: Superlens, negative refractive index and invisibility cloak," *J. Opt.*, vol. 19, no. 8, 2017, Art. no. 084007.

[3] T. Madl, "Patchy proteins form a perfect lens," *Science*, vol. 357, no. 6351, pp. 546–547, 2017.

[4] L. Huang *et al.*, "Experimental demonstration of terahertz metamaterial absorbers with a broad and flat high absorption band," *Opt. Lett.*, vol. 37, no. 2, pp. 154–156, 2012.

[5] S. Han, J.-H. Shin, P.-H. Jung, H. Lee, and B. J. Lee, "Broadband solar thermal absorber based on optical metamaterials for high-temperature applications," *Adv. Opt. Mater.*, vol. 4, no. 8, pp. 1265–1273, 2016.

[6] M. K. Akhlaghi, E. Schelew, and J. F. Young, "Commun waveguide integrated superconducting single-photon detectors implemented as near-perfect absorbers of coherent radiation," *Nat. Commun.*, vol. 6, 2015, Art. no. 8233.

[7] H. Wang, V. Prasad Sivan, A. Mitchell, G. Rosengarten, P. Phelan, and L. Wang, "Highly efficient selective metamaterial absorber for high-temperature solar thermal energy harvesting," *Solar Energy Mater. Solar Cells*, vol. 137, pp. 235–242, 2015.

[8] P. Rufangura, C. Sabah, and J. Alloys Compd, "Wide-band polarization independent perfect metamaterial absorber based on concentric rings topology for solar cells application," *J. Alloys Compounds*, vol. 680, pp. 473–479, 2016.

[9] N. I. Landy, S. Sajuyigbe, J. J. Mock, D. R. Smith, and W. J. Padilla, "Perfect metamaterial absorber," *Phys. Rev. Lett.*, vol. 100, no. 20, 2008, Art. no. 207402.

[10] N. Mishra, D. K. Choudhary, R. Chowdhury, R. K. Kumari, and R. K. Chaudhary, "An investigation on compact ultra-thin triple band polarization independent metamaterial absorber for microwave frequency applications," *IEEE Access*, vol. 5, pp. 4370–4376, 2017.

[11] X. Wang, Q. Wang, G. Dong, Y.-N. Hao, and M. Lei, "Multi-band terahertz metasurface absorber," *Mod. Phys. Lett. B*, vol. 31, 2017, Art. no. 1750354.

[12] V. A. Carey and M. S. Mirotznik, "Multiband absorbers for the long-wave infrared regime," *Appl. Opt.*, vol. 56, no. 30, pp. 8403–8413, 2017.

[13] X.-Y. Duan, S.-Q. Chen, W.-W. Liu, H. Cheng, Z.-C. Li, and J.-G. Tian, "Polarization-insensitive and wide-angle broadband nearly perfect absorber by tunable planar metamaterials in the visible regime," *J. Opt.*, vol. 16, no. 12, pp. 125107–125113, 2014.

[14] D. Wu *et al.*, "Wide-angle, polarization-insensitive and broadband absorber based on eight-fold symmetric SRRs metamaterial," *Opt. Commun.*, vol. 380, pp. 221–226, 2016.

[15] N. T. Q. Hoa, P. H. Lam, and P. D. Tung, "Wide-angle and polarization-independent broadband microwave metamaterial absorber," *Microw. Opt. Technol. Lett.*, vol. 59, no. 5, pp. 1157–1161, 2017.

[16] S.-J. Li, J. Gao, X.-Y. Cao, W.-Q. Li, Z. Zhang, and D. Zhang, "Wideband, thin, and polarization-insensitive perfect absorber based the double octagonal rings metamaterials and lumped resistances," *J. Appl. Phys.*, vol. 116, no. 4, 2014, Art. no. 207402.

[17] Q. Feng, M. Pu, C. Hu, and X. Luo, "Engineering the dispersion of metamaterial surface for broadband infrared absorption," *Opt. Lett.*, vol. 37, no. 11, pp. 2133–2135, 2012.

[18] B.-X. Wang, L.-L. Wang, G.-Z. Wang, W.-Q. Huang, X.-F. Li, and X. Zhai, "A simple design of a broadband, polarization-insensitive, and low-conductivity alloy metamaterial absorber," *Appl. Phys. Exp.*, vol. 7, no. 7, 2014, Art. no. 082601.

[19] J.-F. Chen *et al.*, "High-impedance surface-based broadband absorbers with interference theory," *IEEE Trans. Antennas Propag.*, vol. 63, no. 10, pp. 4367–4374, Oct. 2015.

[20] I. Alexeff, W. L. Kang, M. Rader, and C. Douglass, "A plasma stealth antenna for the US Navy[C]," in *Proc. Int. Conf. IEEE Plasma Sci.*, 1998, Art. no. 277.

[21] X. K. Kong *et al.*, "Microwave tunneling in heterostructures with electromagnetically induced transparency-like metamaterials based on solid state plasma," *Eur. Phys. J.—Appl. Phys.*, vol. 74, no. 3, 2016, Art. no. 30801.

[22] X. K. Kong, J. J. Mo, Z. Y. Yu, W. Shi, and H. M. Li, "Reconfigurable designs for electromagnetically induced transparency in solid state plasma metamaterials with multiple transmission windows," *Int. J. Mod. Phys. B*, vol. 30, no. 14, 2016, Art. no. 1650070.

[23] F. Xue, S. B. Liu, H. F. Zhang, Y. D. Wen, and X. K. Kong, "A novel reconfigurable electromagnetically induced transparency based on S-PINs," *Int. J. Mod. Phys. B*, vol. 32, no. 3, 2018, Art. no. 1850030.